Pressure-induced structural and magnetic phase transitions in ordered and disordered equiatomic FeCo

R. Torchio,[1] Y. O. Kvashnin,[1] C. Marini,[1] O. Mathon,[1] G. Garbarino,[1] M. Mezouar,[1] J. P. Wright,[1] P. Bruno,[1] L. Genovese,[2] F. Baudelet,[3] C. Meneghini,[4] S. Mobilio,[4] N. A. Morley,[5] M. R. J. Gibbs,[5] and S. Pascarelli[1]

[1]*European Synchrotron Radiation Facility, 6 Rue Jules Horowitz, BP220, 38043 Grenoble Cedex, France*

[2]*Laboratoire de Simulation Atomistique, SP2M, UMR-E CEA/UJF-Grenoble 1, INAC, Grenoble F-38054, France*

[3]*Synchrotron SOLEIL, L'Orme des Merisiers, Saint-Aubin, BP 48, 91192 Gif-sur-Yvette, France*

[4]*Dipartimento di Scienze, ROMA TRE, Via della Vasca Navale 84, Rome, Italy*

[5]*Department of Materials Science and Engineering, University of Sheffield, Sheffield, United Kingdom*

(Received 20 June 2013; published 15 November 2013)

The magnetic and structural phase diagram of equiatomic FeCo has been studied up to 45 GPa using *K*-edge x-ray magnetic circular dichroism, x-ray absorption near edge spectroscopy, x-ray diffraction, and supporting density-functional-theory-based calculations. FeCo foils with different degrees of chemical order were obtained by magnetron sputtering. Our results show that $Fe_{0.5}Co_{0.5}$ undergo the bcc ferromagnetic to hcp nonferromagnetic transition in the 30–45 GPa pressure range. Interestingly, the chemical order, i.e., the relative arrangements of Fe and Co atoms, plays a major role in affecting the high-pressure structural and magnetic phase diagram of these alloys. This result is confirmed by first-principles modeling of different structures of equiatomic FeCo alloy. Moreover, the total-energy analysis reveals a strong competition between different magnetic hcp states upon compression. A possible emergence of antiferromagnetism is emphasized and requires further experimental investigation.

DOI: 10.1103/PhysRevB.88.184412 PACS number(s): 75.50.Bb, 61.50.Ks, 61.05.cj

I. INTRODUCTION

Iron cobalt alloys constitute an interesting class of soft magnetic materials being widely employed in technological applications where high magnetic flux densities are required, such as data storage, high-performance transformers, and pole tips for high-field magnets.[1,2] Thanks to their unique combination of high-saturation magnetization, high Curie temperatures, good permeability, considerable mechanical strength, and excellent performance-to-weight ratio, they have been considered for applications in a new generation of aircraft.[3]

The magnetic properties of the transition metals mainly arise from the partially filled spin-polarized 3*d* band, which in turn is related to their crystallographic structure and chemical nature. An understanding of the relationship between the structural, magnetic, and chemical properties of iron-cobalt alloys addresses fundamental questions also because they fall into the interesting category of ordered alloys (see Ref. 2 for a general review). Indeed, the relative distributions of the atomic species over the lattice sites add extra degrees of freedom to the atomic correlations and band filling,[4] thus giving rise to an ample variety of peculiar effects.

Because of their similar electronic structure and atomic volumes, Fe and Co mix together to form alloys, $Fe_{1-x}Co_x$, in the whole concentration range $0 < x < 1$. The structural and magnetic phase diagram of the $Fe_{1-x}Co_x$ system has been extensively investigated in the literature as a function of composition and temperature.[5–17] At room temperature, the end members have different structure, that is, Fe bcc and Co hcp. The crystallographic structure of the alloys remains bcc up to about $x = 0.75$, where the hcp phase stabilizes;[5] in the $x \in (0.9; 1)$ range, fcc, double hcp, and hcp structures have been reported.[6]

$Fe_{1-x}Co_x$ alloys are ferromagnetic (FM) at ambient conditions in the whole composition range and show the highest saturation magnetization (M_S) of all known magnetic alloys. The M_S of $Fe_{1-x}Co_x$ alloys has a nonlinear trend as a function of Co concentration with a maximum around $x = 0.3$.[18,19] Polarized neutron diffraction data demonstrate that this nonlinearity is due to the increasing Fe moment, from $2.2\mu_B$ in pure bcc Fe to approximately $3\mu_B$ beyond $x = 0.5$, whereas the local magnetic moment on Co remains nearly constant at around $1.7\mu_B$.[20]

Great attention is devoted to the role of chemical order and order transition:[2] in nearly equiatomic alloys [$x \in (0.3; 0.75)$], below 730 °C, the bcc phase orders to a CsCl-type structure (α'). Here the atoms of one species (say Fe atoms) are located at the cube center, while the atoms of the other species (Co atoms) stay at the cube corners so that each atom-type is coordinated by eight atoms of the other type and the lattice thus changes from bcc to simple cubic. An increase in the lattice parameter[5,21,22] and in the magnetic moment[22,23] is associated to the ordering reaction.

The application of pressure is an effective tool to understand the complex interplay between electronic, structural, and magnetic degrees of freedom, which characterizes the 3*d* metals. By directly squeezing the interatomic distances, it allows one to modify the band width and density of states at the Fermi level, providing additional information on the electronic structure. The structural and magnetic phase diagram of FeCo under high pressure is particularly fascinating because of the very different behavior of the pure components: compressed iron undergoes a transition at 13 GPa from the bcc α phase to the hcp ϵ phase structure, losing its ferromagnetism.[24,25] On the other hand, Co remains ferromagnetic up to around 120 GPa and undergoes a transition from the hcp to the fcc structure in the 100–150 GPa range.[26–28] Adding Co to iron up to $x = 0.5$ stabilizes the bcc phase, raising the pressure of the structural bcc-to-hcp transition.[29] However,

the high-pressure magnetic phase diagram of $Fe_{1-x}Co_x$ is largely unexplored. Preliminary results[30] pointed out that compressed bcc $Fe_{0.5}Co_{0.5}$ alloys undergo the bcc FM to hcp non-FM transition, just like in pure iron, but at higher pressures in the 30–40 GPa range. The enhanced stability of the FM bcc structure under pressure, with respect to pure Fe, can be related to the strong ferromagnetism of FeCo at this concentration,[31] which follows from the filling of the majority band.[32] Nevertheless, the mechanisms stabilizing the magnetic order against applied pressure require deeper investigation, in particular aimed at understanding the role played by the chemical order and Fe-Co interactions. Therefore, we present here an accurate study on equiatomic $Fe_{0.5}Co_{0.5}$ alloys deposited by sputtering with different degrees of chemical order, combining Fe and Co *K*-edge x-ray absorption near edge structure (XANES), x-ray magnetic circular dichroism (XMCD), synchrotron radiation x-ray diffraction (XRD), and supporting DFT (density functional theory) calculations.

Our results show that the chemical order, which can be tailored by a proper synthesis route, influences significantly the high-pressure magnetic and structural phase diagram of $Fe_{0.5}Co_{0.5}$ alloys.

II. EXPERIMENT

The $Fe_{0.5}Co_{0.5}$ ground-state structure is the chemically ordered cubic CsCl type. Since the ordering reaction is very fast, chemically disordered phases are generally obtained by applying high quenching rates, greater than 4000 °C/s,[22] in order to freeze the structure in a metastable state. Recent studies on sputtered thin Fe-Ga films[33] have shown that by properly tuning the deposition parameters, the sputtering technique can mimic such high cooling rates, providing highly disordered alloy films. In fact, a high deposition rate coupled with low (ambient) substrate temperature prevents significant mobility of the atoms on the substrate.

Homogeneous films of polycrystalline $Fe_{0.5}Co_{0.5}$ about 5 μm thick were synthesized by radio frequency magnetron sputtering deposition[34] using a 50:50 Fe:Co target from Goodfellow. The films were grown on glass substrates passivated with a very thin Al underlayer (less than 20 nm thick). The sputtering power was between 100 and 250 W, with a target-substrate separation of $D = 60$ mm, and total deposition time was 6 h. A part of the pristine film was annealed up to 350 °C in vacuum for 24 h: the high temperature enhances the ion mobility, thereby favoring the structural rearrangement toward chemical order.

Crystallographic (long-range structure), atomic (local structure), and magnetic information as a function of pressure in the 0–45 GPa range was obtained, combining state-of-the-art XRD, XANES, and XMCD techniques. Synchrotron radiation XRD is used to probe the crystallographic structure and long-range chemical order. Fe and Co *K*-edge XANES and XMCD, which are collected simultaneously as unpolarized and polarized x-ray absorption, are sensitive to the local structure and magnetism around the absorber.

Angle-resolved XRD measurements were performed at ID27 (Ref. 35) and ID11 beam lines at the European Synchrotron Radiation Facility (ESRF). XANES-XMCD measurements were carried out at the Co ($E_0 = 7709$ eV) and Fe ($E_0 = 7112$ eV) *K* edges at the energy-dispersive x-ray absorption synchrotron beam lines: ODE (Ref. 36) (SOLEIL synchrotron facility) and ID24 (Ref. 37) (ESRF).

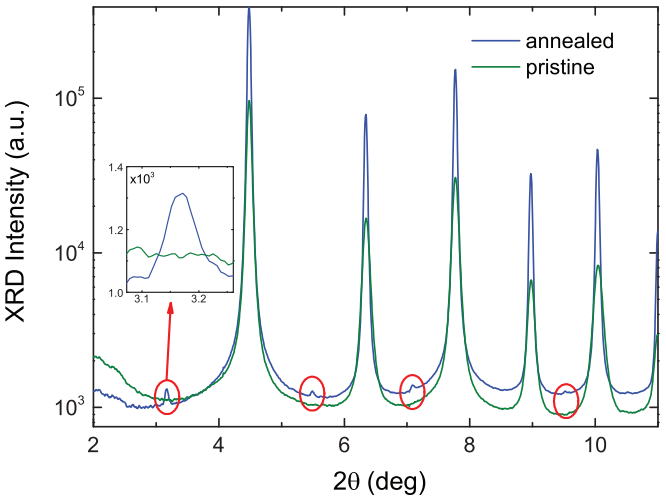

FIG. 1. (Color online) Ambient-condition diffraction patterns of pristine (green line) and annealed (blue line) $Fe_{0.5}Co_{0.5}$ samples. Superlattice reflections (red circles) from the ordered CsCl-type phase are evident in the annealed sample pattern, while they are absent in the pristine film one.

Samples for high-pressure XRD measurements were charged in a Le Toullec diamond anvil cell (DAC)[38] using He as a pressure transmitting medium. Samples for the XANES-XMCD measurements were prepared by charging 1–2 layers of $Fe_{0.5}Co_{0.5}$ film into a nonmagnetic DAC of the Chervin type[39] using silicone oil as a pressure transmitting medium; the applied induction was 0.7 and 1.3 T at ID24 and ODE, respectively. The pressure was monitored with the ruby fluorescence technique;[40] in order to evaluate the pressure gradients, 2–3 ruby spheres were placed at different positions in each DAC.

X-ray diffraction provides long-range (crystallographic) structural and chemical order information. In fact, the simple cubic CsCl symmetry of ordered $Fe_{1-x}Co_x$ alloys gives rise to x-ray diffraction peaks that are forbidden in bcc structure. These peaks are feeble due to the weak difference between Fe and Co scattering factors. The high-quality diffraction spectra collected at ID11 allow one to detect weak reflections in the annealed sample patterns clearly ascribed to a simple cubic superlattice (Fig. 1), while these peaks are absent in the pristine films. This demonstrates that the pristine samples are chemically disordered and that the annealing, as expected, promotes chemical order.

The analysis of the diffractograms (Rietveld refinement analysis) reveals that the lattice parameter of the annealed sample is approximately 0.2% larger than that of the pristine sample (see Table I). This is a further signature of a major degree of chemical order[5,21,22] in annealed $Fe_{0.5}Co_{0.5}$ with respect to the pristine film and demonstrates the efficiency of the preparation route to synthesize chemically disordered FeCo films.

Unfortunately, it is not possible to extract precise information about the degree of chemical order—i.e., the order

TABLE I. Structural parameters for pristine and annealed $Fe_{0.5}Co_{0.5}$: bcc phase lattice parameter (a bcc), hcp phase lattice parameters ratio (c/a), ambient volume (V_0), volume change (ΔV), bcc phase bulk modulus ($K_0{}^{bcc}$), and its pressure derivative ($K'_0{}^{bcc}$).

$Fe_{0.5}$ $Co_{0.5}$	a bcc (Å)	c/a hcp	V_0 (Å^3/atom)	ΔV (Å^3/atom)	$K_0{}^{bcc}$ (GPa)	$K'_0{}^{bcc}$
Pristine	2.854(2)	1.6074(35)	11.62(2)	0.0354(1)	193(10)	4.5(7)
Annealed	2.860(4)	1.6140(30)	11.69(4)	0.0336(6)	189(7)	4(1)

parameter S, related to the relative intensity of the 100 and 200 reflections[22]—from conventional x-ray measurement, since the diffraction lines of the simple cubic (ordered) lattice are too weak. According to Clegg and co-workers,[22] S can otherwise be estimated from the increasing of the lattice parameter a; in Ref. 22, $\Delta a = 0.07\%$ is found between fully ordered and disordered FeCo alloys. Our observed Δa amounts to 0.2%, suggesting that our samples might be fully ordered and disordered; however, the error in the lattice parameter determination is quite large (about 0.1%).

High-pressure XRD measurements were performed on ID27 to follow the structural evolution across the bcc-hcp transition (Fig. 2). Both samples show the pressure-induced bcc-to-hcp transition. Interestingly, in the pristine sample, the phase transformation occurs and is completed within the 31–36 GPa range, whereas in the annealed sample, it is retarded by around 7 GPa and bcc features remain up to 40 GPa (see the bcc/hcp phase fraction plotted in Fig. 6).

The XRD patterns were analyzed using both a Le Bail[41] fit and Rietveld[42] refinement method using GSAS[43] and DATLAB[44] programs; the structural parameters are summarized in Fig. 3 and Table I. Just like in the elemental iron case, the bcc-hcp transition in $Fe_{0.5}Co_{0.5}$ is a first-order transition, since it is accompanied by a volume change. The c/a ratio of the P-induced hcp structure[45] obtained in the case of the annealed sample is larger with respect to the pristine sample, whereas the transition volume change ΔV is smaller, pointing out that the different degree of chemical order also has an effect on the high-pressure structural properties; on the other hand, the compressibilities remain similar.

In Fig. 4, we compare our data to previous literature data covering the lower Co concentration range.[29,47,48] The ambient bcc lattice parameter a, the c/a ratio of the pressure-induced hcp structure, and the transition pressure obtained for the annealed sample are in quite good agreement with previous studies. The samples in the cited references were produced by melting mixes of the pure components and were also annealed, and therefore likely chemically ordered. This proves that the ordering effect produced by the annealing gives rise to reproducible structural properties even when the base synthesis is different (melting or sputtering).

We note that the compressibility value is outside of the trend reported by Papantonis;[29] however, the values in Ref. 29 were obtained from Birch-Murnaghan fits over very few (from 3 to 6) pressure points.

Simultaneous XANES-XMCD measurements provide element-selective information about the local structure and magnetism around the absorbing atoms, respectively. In particular, the observation of a nonzero XMCD signal is an indication of a ferromagnetic state. In Fig. 5, we report the high-pressure XANES and XMCD spectra measured on pristine $Fe_{0.5}Co_{0.5}$ at the Co and Fe K edges. The Fe and Co XANES spectra at room pressure are similar and depict features which are characteristic of the bcc structure.[25] A weak difference between Fe and Co XANES is observed in the pre-edge shoulder (labeled as a in Fig. 5), being better resolved at the Fe edge. The evolution of the XANES features as a function of the applied pressure is also quite alike at the two edges, pointing out a common local structure change: in the 0–30 GPa range, the spectral features in the high-energy region expand, signaling the overall squeezing of the interatomic distances under pressure; the pre-edge shoulder a ($E - E_0 \approx 4$ eV) continuously grows in intensity and becomes sharper; the white line feature b ($E - E_0 \approx 20$ eV) loses intensity; the

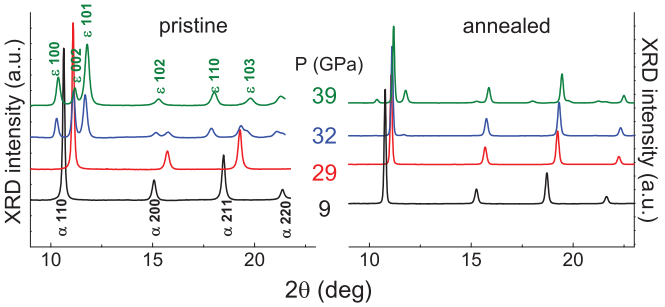

FIG. 2. (Color online) Selection of XRD patterns of pristine (left) and annealed (right) $Fe_{0.5}Co_{0.5}$ as a function of pressure; the bcc (α) and hcp (ϵ) phase reflections are indicated. The comparison clearly shows that the structural transition in the pristine occurs at an earlier stage.

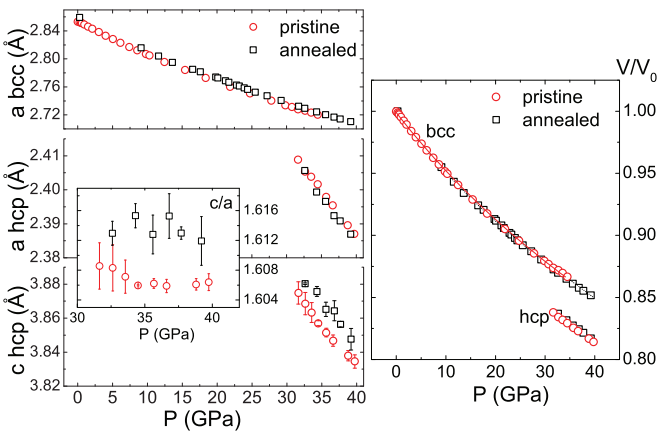

FIG. 3. (Color online) Pressure evolution of the bcc and hcp structural parameters (left) and compression curves (right) of pristine (red empty circles) and annealed (black empty squares) $Fe_{0.5}Co_{0.5}$. Not indicated errors are within the symbols. Solid and dashed lines in the right panel are Birch-Murnaghan fits to the data.

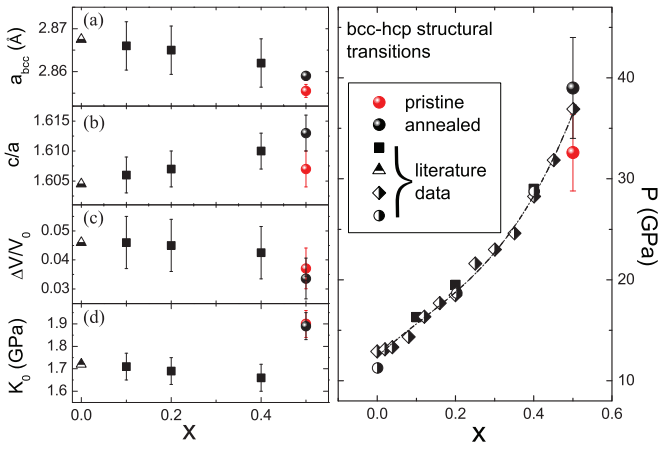

FIG. 4. (Color online) Left: Structural ambient and high-pressure parameters in $Fe_{1-x}Co_x$ for $x \in (0; 0.5)$: (a) ambient a bcc parameter, (b) high-pressure hcp structure c/a ratio, (c) bcc-hcp transition volume change $\Delta V/V_0$, and (d) bcc phase bulk modulus K_0. Right: bcc-hcp transition pressure as a function of concentration x. Black and red full circles are from this work for annealed and pristine samples, respectively; black squares are from Ref. 29; half-filled rhombus, triangle, and circle are from Refs. 47–49, respectively.

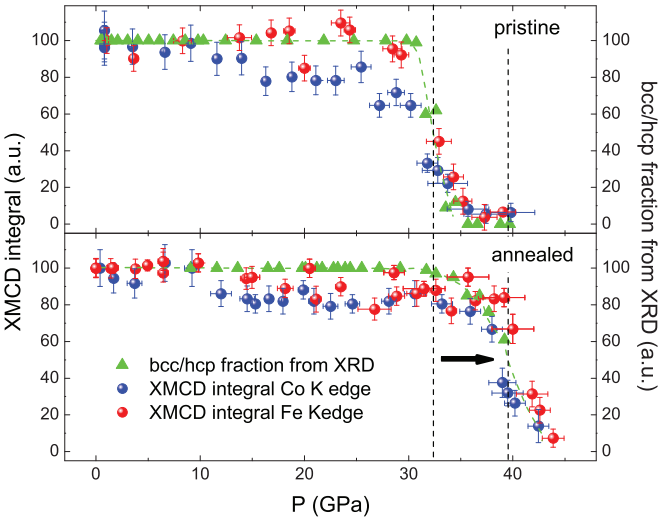

FIG. 6. (Color online) Integral of the XMCD signal at Co and Fe edges (blue and red full circles, respectively) and comparison with bcc/hcp phase fraction from XRD (green full triangle) for the pristine sample (top panel) and annealed sample (bottom panel). The phase fraction error is around 10% and its pressure error is within the symbol size.

double-shaped first oscillation c ($E - E_0 \approx 50$ eV) turns into a single rounded one, while the second and third oscillations d ($E - E_0 \approx 84$ eV) and d' ($E - E_0 \approx 109$ eV) merge into a single broad peak. This is reminiscent of the pure iron case.[25] The hcp structure stabilizes around 36–38 GPa since no further modification can be appreciated above this pressure.

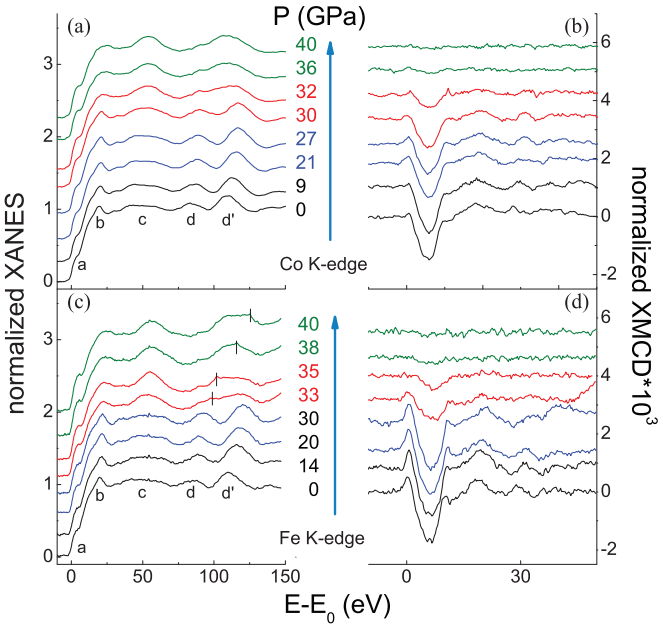

FIG. 5. (Color online) Normalized XANES and XMCD spectra of pristine $Fe_{0.5}Co_{0.5}$ measured at the Co K edge [(a) and (b), respectively] and at the Fe-K edge [(c) and (d), respectively]. In (c), the presence of a diamond glitch is signaled by short lines. The origin of the energy scale is selected at the first inflection point of the absorption edge at ambient pressure.

The XMCD spectra measured at ambient pressure depict some differences between the Fe and Co K edges: the Fe K-edge XMCD main negative peak is deeper than the Co K-edge one, and is accompanied by a pre-edge positive lobe which is almost absent in the Co K-edge XMCD signal. This difference has already been highlighted by Pizzini and co-workers for disordered FeCo alloys:[50] they suggested the main negative peak intensity to be related to the magnetic moment of the absorbing atoms, whereas the presence/absence of the pre-peak was interpreted as due to a different scattering of the photoelectron d components from neighbors around the Co and the Fe absorber. A detailed analysis of the XMCD shape in ordered and disordered FeCo alloys is beyond the scope of this paper and will be treated elsewhere. Compression leads to the decrease of the XMCD signal both at Fe and Co K edges with total extinction occurring in correspondence to the bcc-to-hcp transition, indicating that the high-pressure hcp structure in $Fe_{0.5}Co_{0.5}$ is nonferromagnetic, similarly to the bulk iron case.

In order to relate the magnetic and structural transitions, we compare (Fig. 6) the pressure evolution of the integral of the main XMCD peak (at Fe and Co edges) with that of the bcc/hcp phase fraction as estimated from the XRD Rietveld analysis.[42] In the pristine $Fe_{0.5}Co_{0.5}$ film (Fig. 6, top panel), the sharp decrease of the XMCD signal integral is observed starting from around 30 GPa (Fe and Co edges), at the same pressure in which the XRD data show the onset of the bcc-to-hcp long-range structural transformation, pointing out that the magnetic and structural transition are simultaneous. The same occurs for the annealed sample, but the magnetic and structural transition are delayed by about 7 GPa (Fig. 4, bottom panel). This finding demonstrates that the degree of chemical order, i.e., the relative arrangement of Fe and Co atoms in the alloy lattice, plays a major role in determining the resistance of the bcc-FM phase against applied pressure: the chemically ordered (disordered)

annealed (pristine) sample showing higher (lower) transition pressure.

III. *AB INITIO* MODELING

In order to shed light on the role played by the chemical order on the high-pressure structural and magnetic properties of $Fe_{0.5}Co_{0.5}$, DFT calculations were carried out using the VASP package.[51] In a recent work on pure nickel, some of us have demonstrated that the pressure evolution of *K*-edge XMCD is related to that of the *p*-projected orbital moment, rather than to total spin moment.[52] Such analysis in Ni was possible because of the large stability range of the fcc phase up to very high compression. On the contrary, in the present work, we observe changes in both structural and magnetic properties simultaneously and we need to deal with the competition between different structural and magnetic phases under pressure. The observed dropoff of XMCD is an indication of restoring of the macroscopic time-reversal symmetry, i.e., disappearance of the net magnetic moment. Therefore, for this discussion, we can omit the effects of spin-orbit coupling and rely on classical spin-polarized DFT calculations, which are sufficient to say whether the system has a preference to be ferromagnetic or not under certain external conditions.

The projector augmented wave method was used, with the Perdew-Burke-Ernzerhof exchange-correlation approximation.[53] A 600 eV energy cutoff was chosen to ensure convergence with respect to the basis set, together with a *k*-point sampling equivalent to a length of ≈19 a.u. The enthalpy $H = E_{tot} + PV$, where E_{tot} is total energy, was used as a criterion to establish the most convenient structure as a function of the pressure. The magnetization around Co and Fe atoms was calculated within a Wigner-Seitz radius of 1.3 Å and 1.16 Å, respectively.

Calculation were carried out for the CsCl-type crystal structure of FeCo [Fig. 7(a)], which is the most preferable one from a thermodynamical viewpoint at ambient conditions (see, for example, Ref. 54). Its hcp counterpart, shown in Fig. 7(c), was constructed following the transition path proposed by Burgers.[55,56] In this scenario, the bcc-hcp transformation is of the martensitic type, where two neighboring (110) planes are shifted and sheared, hence forming a proper hcp "*ABAB*" stacking.[57]

In order to study the effect of chemical environment, we have also considered a Zintl-type structure, characterized by each atom being coordinated with four atoms of the same element and four of the other type, hence maximizing the amount of homopolar bonds. Corresponding bcc and hcp crystal structures are shown in Figs. 7(b) and 7(d).

Then, for a given crystalline phase, several magnetic configurations were considered, for instance, high- (low-)spin FM, antiferromagnetic (AFM), and nonmagnetic (NM) states. Note that the list of considered states is actually not exhaustive; in fact, in order to find the magnetic ground state, one has to extract and thoroughly analyze exchange integrals (see Ref. 58), which is beyond the scope of the present study. Starting from a particular spin structure, the Bravais vectors of the lattice were optimized to provide a certain value of isotropic stress. We report that the assumed magnetic state strongly influences

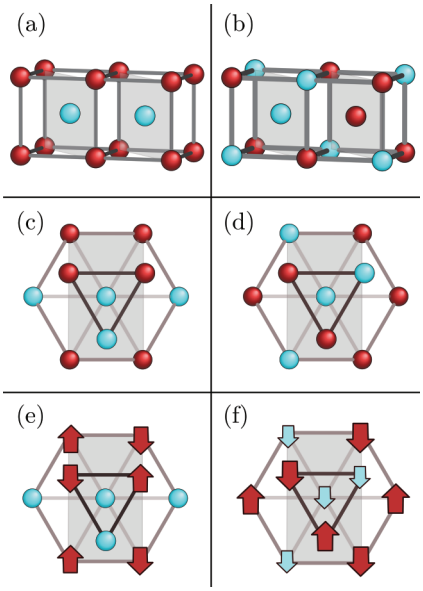

FIG. 7. (Color online) Considered crystal structures of equiatomic FeCo alloy. The (a) bcc CsCl and (b) Zintl phases. Their hcp counterparts are depicted in (c) and (d), respectively. Vinous and cyan (dark and light) spheres represent two atomic sorts (Fe and Co). Shaded areas indicate the (110) planes in bcc structures, which become (0001) and (0002) ones in the hcp states. These planes are represented by a hexagon and a triangle in the hcp phase. Suggested spin configurations in high-pressure (e) hcp CsCl and (f) Zintl phases, respectively.

corresponding crystal structures. In particular, strong deviations of the c/a ratio in the hcp phase is emphasized. It is also worth noting that the comparison of total energies of different magnetic structures is rather complex; in fact, it involves energy differences of the order of the interatomic exchange (typically several meV), which are much smaller than those associated with the atomic displacements (∼eV). The typical decrease of magnetic-moment magnitudes under pressure further reduces the energy scale and complicates the analysis.

The comparison between the calculated enthalpies for the different phases, shown in Fig. 8 (top panel), confirms that the ferromagnetic CsCl-type bcc structure is energetically the most preferable at ambient pressure. Interestingly, when the spin polarization is neglected, the hcp structure becomes a preferable one at equilibrium. Hence, it is magnetism that plays a key role in the stabilization of the bcc phase, as was already pointed out in several prior studies.[54,59–61] However, as the applied pressure is raised, the system's tendency for compact atomic arrangement starts to dominate, leading the hcp phases to have lower enthalpies at ≈33 GPa. At this point, several magnetic configurations are almost degenerate in energy, due to the reasons mentioned above. Among the studied spin configurations in the hcp structure, the AFM one, shown in Fig. 7(e), shows the lower enthalpy. Notably, in this state, Co ions, surrounded by iron moments pointing "up" and "down," turn out to be nonmagnetic. Thus, Co exhibits a Stoner-like (nonlocal) magnetism behavior.

Similarly, the occurrence of antiferromagnetism in the high-pressure hcp phase of pure iron was suggested by several research groups.[62,63] The AFM exchange interactions (J)

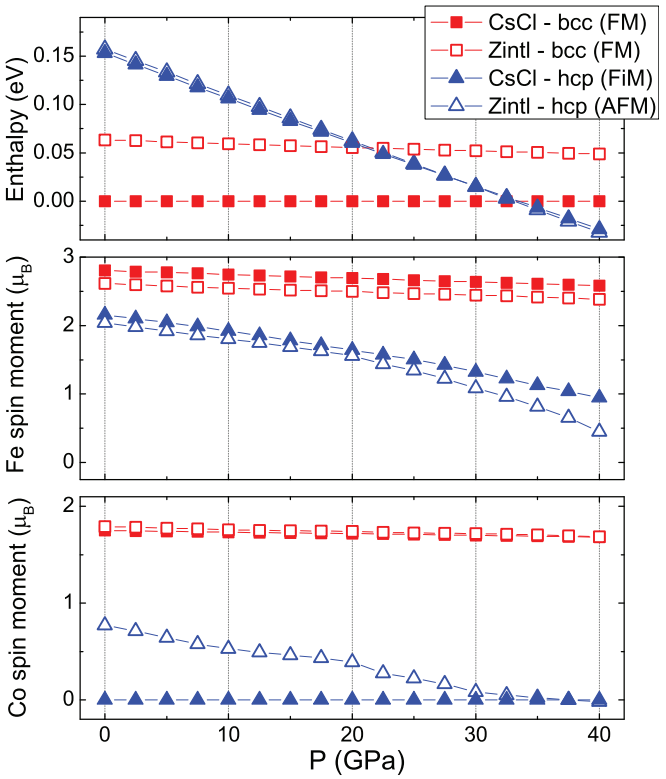

FIG. 8. (Color online) Calculated relative enthalpies per atom (top panel) and saturated magnetic moments (bottom panels) in various phases of equiatomic FeCo alloy. The enthalpy of the CsCl-bcc FM phase is taken as reference.

between nearest-neighbor Fe atoms are suspected to be the origin of stabilization of this state.[64] However, the triangular lattice is frustrated for such sign of J, thus it might give rise to noncollinear spin arrangements.[65]

In the case of FeCo, total-energy analysis of various magnetic states suggests the same sign of Fe-Fe interactions. However, differently from the case of pure iron, the presence of another atomic sort allows one to reduce the symmetry and remove the frustration. Indeed, in the CsCl hcp phase, Co atoms become NM, and therefore do not participate in magnetic couplings, and all Fe-Fe interactions can be satisfied within the geometry shown in Fig. 7(e).

As far as the Zintl phase is concerned, the martensitic bcc-hcp transformation is predicted to happen at a lower pressure, as compared with CsCl structure, i.e., around 22 GPa. According to our results, this phase also shows a tendency to antiferromagnetism among nearest-neighbor Fe atoms. However, the environment of Co atoms is less symmetrical in this case and we found that it can acquire a nonzero magnetization. These Co moments show a preference for FM ordering and thus we found a ferrimagnetic (FiM) state, shown in Fig. 7(f), to have lower enthalpy than other FM and AFM states. Here, the net Fe magnetization is compensated, whereas the one originated from Co is finite. It equals $\approx 0.77 \mu_B$ per atom at ambient pressure and gradually decreases upon volume compression.

In both hcp CsCl and Zintl phases, as a consequence of the small (or absent) Co magnetization, Fe is pushed back to the "weak ferromagnet" limit, and thus its magnetic moment becomes more sensitive to the application of pressure (Fig. 8) because both spin-up and spin-down electrons are exposed to the effect of pressure application.

The higher resistance to compression of the ordered CsCl-bcc FM phase is in agreement with our experimental observation since the major degree of chemical order, produced by the annealing, pushes the magnetic/structural transition to higher pressures (Fig. 6). Moreover the optimized hcp structures described above are characterized by a c/a ratio equal to ≈ 1.6, which compares favorably to XRD data. The bcc CsCl phase is more stable than the Zintl one in the entire pressure range, most likely because iron acquires a greater magnetic moment in the former case (Fig. 8, middle panel). Since the energy gain due to the presence of the magnetization (M) is proportional to M^2, this contribution is larger in the CsCl phase and can qualitatively explain its higher stability.

Looking more in detail, we notice that the comparison with experimental results is quite satisfactory for the ordered phase. In fact, in the CsCl-type structure, the pressure at which the hcp phase becomes favorite ($\approx$35 GPa; Fig. 8, top panel) corresponds to the onset of the experimentally observed bcc-hcp transition in the ordered annealed $Fe_{0.5}Co_{0.5}$ film (Fig. 6, bottom panel). As to the magnetic state, since the XMCD is only sensitive to the existence of a net magnetic moment, both the AFM ordering of the Fe moments and the NM of Co moments predicted in the hcp phase of CsCl type are compatible with the zero XMCD signal observed at the Fe and Co edge, respectively.

In the Zintl-type structure, the predicted bcc-hcp transition pressure ($\approx$22 GPa; Fig. 8, top panel) is lower than the observed transition onset in the disordered pristine film (around 30 GPa; Fig. 6, top panel). Moreover, the suggested FiM ordering would give a nonzero XMCD signal at the Co K edge at this transition pressure, which would then rapidly drop to zero by 30 GPa. On a quantitative level, the Zintl-type structure, characterized by the maximal number of homopolar bonds around each atom, does not describe correctly the effect of disorder and therefore it is not surprising that the transition pressures are so different. Therefore, we anticipate that use of, for instance, the coherent potential approximation (CPA)[66] in the calculations can improve the results for the disordered specimen. Moreover, the actual pristine sample may be in an intermediate situation characterized by a low but nonzero degree of chemical order, invisible to XRD because of the short coherence length of ordered domains and the closely similar scattering factors weakening the superlattice reflections. Indeed, this discordance stimulates further experimental and theoretical work.

Also the predicted AFM ordering in the high-pressure phases should be addressed and verified experimentally, likely using linear dichroism or Mössbauer spectroscopy.

IV. CONCLUSIONS

The high-pressure magnetic and structural behavior of equiatomic FeCo alloys with different degree of chemical order has been investigated by means of polarized absorption in the near edge region (XMCD-XANES) and XRD. In

addition, first-principles calculations were used to model possible magnetic/structural phases. This study leads to the following conclusions:

(1) The magnetron sputtering technique is able to reproduce the effect of fast quenching, allowing one to prepare chemically disordered FeCo alloys. Chemical order can then be restored by annealing of the samples.

(2) Both sputtered pristine and annealed $Fe_{0.5}Co_{0.5}$ undergo a *P*-induced bcc FM to hcp non-FM phase transition, similarly to pure iron, but at higher compression as a consequence of the stronger ferromagnetism given by the filling of the majority band.

(3) The chemical order (disorder) has a major effect on the high-pressure structural and magnetic response in the equiatomic FeCo alloy. Chemically ordered structures are more resistant to compression than their disordered counterparts, as the structural/magnetic transition is observed at higher pressures: in the pristine (disordered) samples, it occurs within 30–36 GPa, whereas in the annealed samples, it occurs at 35–43 GPa. This statement is supported by the results of DFT-based calculations.

(4) *Ab initio* calculations reveal a competition between several magnetic configurations in the high-pressure hcp phase of $Fe_{0.5}Co_{0.5}$. We report a pronounced tendency to antiferromagnetism among Fe magnetic moments. However, the bcc-hcp transition path and magnetic state in the high-pressure hcp phase are not conclusive and require further experimental studies.

[1] R. S. Sundar and S. C. Deevi, Int. Mater. Rev. **50**, 157 (2005).
[2] T. Sourmail, Prog. Mater. Sci. **50**, 816 (2005).
[3] R. E. Quigley (unpublished).
[4] R. H. Victora and L. M. Falicov, Phys. Rev. B **30**, 259 (1984)
[5] W. C. Ellis and E. S. Greiner, Trans. Am. Soc. Met., 415 (1941).
[6] T. Wakiyama, AIP Conf. Proc. **2**, 921 (1973).
[7] T. Nishizawa and K. Ishida, *Binary Alloy Phase Diagrams*, 2nd ed. (ASM, Metal Park, OH, 1990), Vol. 2, p. 1186.
[8] L. Kaufman and H. Nesor, Z. Metallkd. **64**, 249 (1973).
[9] G. Inden and W. Pepperhoff, Z. Metallkd. **81**, 770 (1990).
[10] M. Hillert and M. Jarl, CALPHAD: Comput. Coupling Phase Diagrams Thermochem. **2**, 227 (1978).
[11] F. Guillermet, High Temp.–High Pressures **19**, 477 (1987).
[12] C. Colinet, G. Inden, and R. Kikuchi, Acta Metall. Mater. **41**, 1109 (1993).
[13] C. Colinet and A. Antoni-Zdziobek, JOM **52**, 26 (2000).
[14] I. Ohnuma, O. Ikeda, R. Kainuma, B. Sundman, and K. Ishida, Z. Metallkd. **89**, 847 (1998).
[15] I. Ohnuma, H. Enokia, O. Ikeda, R. Kainuma, H. Ohtani, B. Sundman, and K. Ishida, Acta Mater. **50**, 379 (2002).
[16] C. Petrillo and F. Sacchetti, Solid State Commun. **89**, 471 (1994).
[17] C. Petrillo and F. Sacchetti, J. Magn. Magn. Mater. **133**, 90 (1994).
[18] P. Weiss and R. Forrer, Ann. Phys. **12**, 279 (1929).
[19] D. I. Bardos, J. Appl. Phys. **40**, 1371 (1961).
[20] M. F. Collins and J. B. Forsyth, Philos. Mag. **8**, 401 (1963).
[21] R. M. Bozorth, *Ferromagnetism* (IEEE, New York, 1993).
[22] D. W. Clegg and R. A. Buckley, J. Metal. Sci. **7**, 48 (1973).
[23] J. E. Goldman and R. Smoluchowski, Phys. Rev. **75**, 310 (1949).
[24] D. Bancroft, E. L. Peterson, and S. Minshall, J. Appl. Phys. **27**, 291 (1956).
[25] O. Mathon, F. Baudelet, J. P. Itie, A. Polian, M. d'Astuto, J. C. Chervin, and S. Pascarelli, Phys. Rev. Lett. **93**, 255503 (2004).
[26] R. Torchio, A. Monza, F. Baudelet, S. Pascarelli, O. Mathon, E. Pugh, D. Antonangeli, and J. P. Itie, Phys. Rev. B **84**, 060403(R) (2011).
[27] N. Ishimatsu, N. Kawamura, H. Maruyama, M. Mizumaki, T. Matsuoka, H. Yumoto, H. Ohashi, and M. Suzuki, Phys. Rev. B **83**, 180409(R) (2011).
[28] C. S. Yoo, H. Cynn, P. Söderlind, and V. Iota, Phys. Rev. Lett. **84**, 4132 (2000).
[29] D. Papantonis and W. A. Bassett, J. Appl. Phys. **48**, 3374 (1977).
[30] R. Torchio, S. Pascarelli, O. Mathon, C. Marini, S. Anzellini, P. Centomo, C. Meneghini, S. Mobilio, N. A. Morley, and M. R. J. Gibbs, High Pressure Res. **31**, 148 (2011).
[31] V. Iota, J. H. P. Klepeis, C. S. Yoo, J. Lang, D. Haskel, and G. Srajer, Appl. Phys. Lett. **90**, 042505 (2007).
[32] K. Schwarz, P. Mohn, P. Blaha, and J. Kubler, J. Phys. F: Met. Phys. **14**, 2659 (1984).
[33] A. Javed, T. Szumiata, N. A. Morley, and M. R. J. Gibbs, Acta Mater. **58**, 4003 (2010).
[34] M. D. Cooke, M. R. J. Gibbs, and R. F. Pettifer, J. Magn. Magn. Mater. **237**, 175 (2001).
[35] M. Mezouar, W. A. Crichton, S. Bauchau, F. Thurel, H. Witsch, F. Torrecillas, G. Blattmann, P. Marion, Y. Dabin, J. Chavanne, O. Hignette, C. Morawe, and C. Borel, J. Synchrotron Radiat. **12**, 659 (2005).
[36] F. Baudelet, Q. Kong, L. Nataf, J. D. Cafun, A. Congeduti, A. Monza, S. Chagnot, and J. P. Iti, High Pressure Res. **31**, 136 (2011).
[37] S. Pascarelli, O. Mathon, M. Munoz, T. Mairs, and J. Susini, J. Synchrotron Radiat. **13**, 351 (2006).
[38] R. Le Toullec, J. P. Pinceaux, and P. Loubeyre, High Pressure Res. **1**, 77 (1988).
[39] J. C. Chervin, B. Canny, J. M. Besson, and Ph. Pruzan, Rev. Sci. Instrum. **66**, 2595 (1995).
[40] H. K. Mao, J. Xu, and P. Bell, J. Geophys. Res. **91**, 4673 (1986).
[41] A. Le Bail, H. Duroy and J. L. Fourquet, Mater. Res. Bull. **23**, 447 (1988).
[42] H. M. Rietveld, Acta Crystallogr. **22**, 151 (1967).
[43] A. C. Larson and R. B. Von Dreele, General Structure Analysis System (GSAS), Los Alamos National Laboratory, Report No. LAUR 86-748, 1994 (unpublished).
[44] K. Syassen, computer code DATLAB (Max Planck Institute, Stuttgart, Germany, 2003).
[45] In the case of the c/a ratio, we have to keep in mind that since the bcc-hcp transition is not completed in the annealed sample case, the observed c/a ratio may not be stable. In fact, when the two phases are present, interfacial strain can affect the c/a value.[46]
[46] F. M. Wang and R. Ingalls, Phys. Rev. B **57**, 5647 (1998).
[47] T. R. Loree, C. M. Fowler, E. G. Zukas, and F. S. Minshall, J. Appl. Phys. **37**, 1918 (1966).
[48] F. P. Bundy, Rev. Sci. Instrum. **46**, 1318 (1975).

[49]T. Takahashi, W. A. Basset, and H. K. Mao, J. Geophys. Res. **73**, 4717 (1968).
[50]S. Pizzini, A. Fontaine, E. Dartyge, C. Giorgetti, F. Baudelet, J. P. Kappler, P. Boher, and F. Giron, Phys. Rev. B **50**, 3779 (1994).
[51]G. Kresse and J. Furthmuller, Comput. Mater. Sci. **6**, 15 (1996).
[52]R. Torchio, Y. O. Kvashnin, S. Pascarelli, O. Mathon, C. Marini, L. Genovese, P. Bruno, G. Garbarino, A. Dewaele, F. Occelli, and P. Loubeyre, Phys. Rev. Lett. **107**, 237202 (2011).
[53]J. P. Perdew, K. Burke, and M. Ernzerhof, Phys. Rev. Lett. **77**, 3865 (1996).
[54]A. Diaz-Ortiz, R. Drautz, M. Fahnle, H. Dosch, and J. M. Sanchez, Phys. Rev. B **73**, 224208 (2006).
[55]W. G. Burgers, Physica **1**, 561 (1934).
[56]M. Ekman, B. Sadigh, K. Einarsdotter, and P. Blaha, Phys. Rev. B **58**, 5296 (1998).
[57]In principle, transformations involving diffusion of some atoms cannot be omitted. However, in this case, the final state is likely to be separated from the initial state by rather high energy barriers. This issue requires additional investigations and is beyond the scope of this paper.
[58]J. M. MacLaren, T. C. Schulthess, W. H. Butler, R. Sutton, and M. McHenry, J. Appl. Phys. **85**, 4833 (1999).
[59]J. Kudrnovský, I. Turek, A. Pasturel, R. Tetot, V. Drchal, and P. Weinberger, Phys. Rev. B **50**, 9603 (1994).
[60]I. A. Abrikosov, P. James, O. Eriksson, P. Soderlind, A. V. Ruban, H. L. Skriver, and B. Johansson, Phys. Rev. B **54**, 3380 (1996).
[61]P. Söderlind, R. Ahuja, O. Eriksson, J. M. Wills, and B. Johansson, Phys. Rev. B **50**, 5918 (1994).
[62]M. Friak and M. Sob, Phys. Rev. B **77**, 174117 (2008).
[63]G. Steinle-Neumann, R. E. Cohen, and L. Stixrude, J. Phys.: Condens. Matter **16**, S1109 (2004); G. Steinle-Neumann, L. Stixrude, and R. E. Cohen, Proc. Natl. Acad. Sci. USA **101**, 33 (2004).
[64]S. Khmelevskyi, A. V. Ruban, and P. Mohn, Physica C **647**, 460 (2007).
[65]R. Lizárraga, L. Nordström, O. Eriksson, and J. Wills, Phys. Rev. B **78**, 064410 (2008).
[66]P. Soven, Phys. Rev. **156**, 809 (1967).